# Complete Protection of O 2 -Sensitive Catalysts in Thin Films

Huaiguang Li, Darren Buesen, Sébastien Dementin, Christophe Léger, Vincent Fourmond, Nicolas Plumere

JACS JOURNAL OF THE AMERICAN CHEMICAL SOCIETY

Article

Cite This: J. Am. Chem. Soc. 2019, 141, 16734−16742

pubs.acs.org/JACS

# Complete Protection of $O_2$-Sensitive Catalysts in Thin Films

Huaiguang Li,[†] Darren Buesen,[†] Sébastien Dementin,[‡] Christophe Léger,*[,‡] Vincent Fourmond,*[,‡] and Nicolas Plumeré*[,†]

[†]Center for Electrochemical Sciences (CES), Faculty of Chemistry and Biochemistry, Ruhr University Bochum, Universitätsstr. 150, D-44780 Bochum, Germany

[‡]CNRS, Aix-Marseille Université, Laboratoire de Bioénergétique et Ingénierie des Protéines, Marseille, France

Supporting Information

**ABSTRACT:** Energy conversion schemes involving dihydrogen hold great potential for meeting sustainable energy needs, but widespread implementation cannot proceed without solutions that mitigate the cost of rare metal catalysts and the $O_2$ instability of biological and bioinspired replacements. Recently, thick films (>100 $\mu$m) of redox polymers were shown to prevent $O_2$ catalyst damage but also resulted in unnecessary catalyst load and mass transport limitations. Here we apply novel homogeneous thin films (down to 3 $\mu$m) that provide protection from $O_2$ while achieving highly efficient catalyst utilization. Our empirical data are explained by modeling, demonstrating that resistance to $O_2$ inactivation can be obtained for nonlimiting periods of time when the optimal thickness for catalyst utilization and current generation is achieved, even when using highly fragile catalysts such as the enzyme hydrogenase. We show that different protection mechanisms operate depending on the matrix dimensions and the intrinsic catalyst properties and can be integrated together synergistically to achieve stable $H_2$ oxidation currents in the presence of $O_2$, potentially enabling a plethora of practical applications for bioinspired catalysts under harsh oxidative conditions.

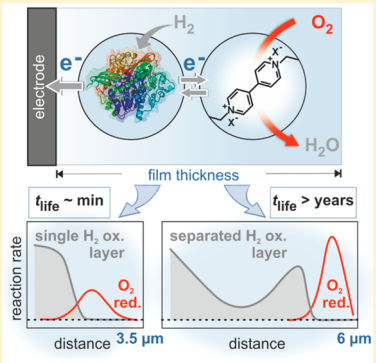


## INTRODUCTION

The need for a global implementation of sustainable energy schemes drives the search for cost-effective clean energy sources and storage technologies. In energy conversion processes, catalysts based on earth-abundant elements are needed to replace rare-metal-based anodes such as platinum for the efficient generation and conversion of key energy carriers such as dihydrogen. Recent advances in molecular catalysis,[1−5] inspired by the understanding of enzymes,[6] have raised expectations for the development of cheap, highly active catalysts. However, in contrast with materials based on noble metals, molecular and biological systems easily deactivate when used under operating conditions that are relevant for real-world applications.[7] One particular challenge is an oxidative degradation, as observed for molecular catalysts for $H_2$ oxidation[8] and enzymes capable of $H_2/H^+$ interconversion such as hydrogenase ($H_2$ase, Figure 1A).[9] Because the strict exclusion of $O_2$ over a long-term operation in water splitting cells or fuel cells is impossible, due to membrane crossovers or contamination by $O_2$ from air, the current paradigm in chemical energy conversion is to increase the resistance of the catalyst to $O_2$-induced damage.

However, recent developments in protective matrices have also allowed the possibility of using $O_2$-sensitive catalysts in an oxidative environment. Such matrices consist of a film of redox polymer deposited onto an electrode and embedding a catalyst such as a hydrogenase. Matrix-bound viologens (Figure 1B) can serve as redox moieties, owing to their ability to shuttle electrons within the film, their fast charge exchange with hydrogenases, their matching redox potential for $H_2$ oxidation, and, most importantly, their catalytic activity for $O_2$ reduction. These properties allow for the diversion of electrons generated from $H_2$ oxidation toward the reduction of the $O_2$ molecules that penetrate the film at the matrix/solution interface,[10−12] so that the hydrogenase molecules immobilized within the film are shielded from $O_2$ (labels (1) in Figures 1D and 1F). Hence the enzymes do not experience the oxidative conditions of an operating fuel cell and thus maintain their activity under conditions that are relevant for practical applications. This breakthrough in catalyst protection, initially developed for electrocatalytic $H_2$ oxidation with a NiFe hydrogenase,[10] has since been applied to various other catalysts.[12−15]

However, the actual use of such protective matrices has been limited because this protection mechanism was demonstrated only for thick films (>100 $\mu$m), in which the $H_2$ oxidation reaction layer that sends electrons toward the electrode (electrocatalytic layer) is very thin. Hence, the vast majority of the catalyst does not contribute to current generation (Figure 1E, top). Moreover, the catalytic performances of the film are suboptimal because the $H_2$ oxidation current is limited by the $H_2$ transport within the film (Figure 1E, bottom). Therefore, thick films provide protection at the cost of

Received: June 26, 2019
Published: September 16, 2019

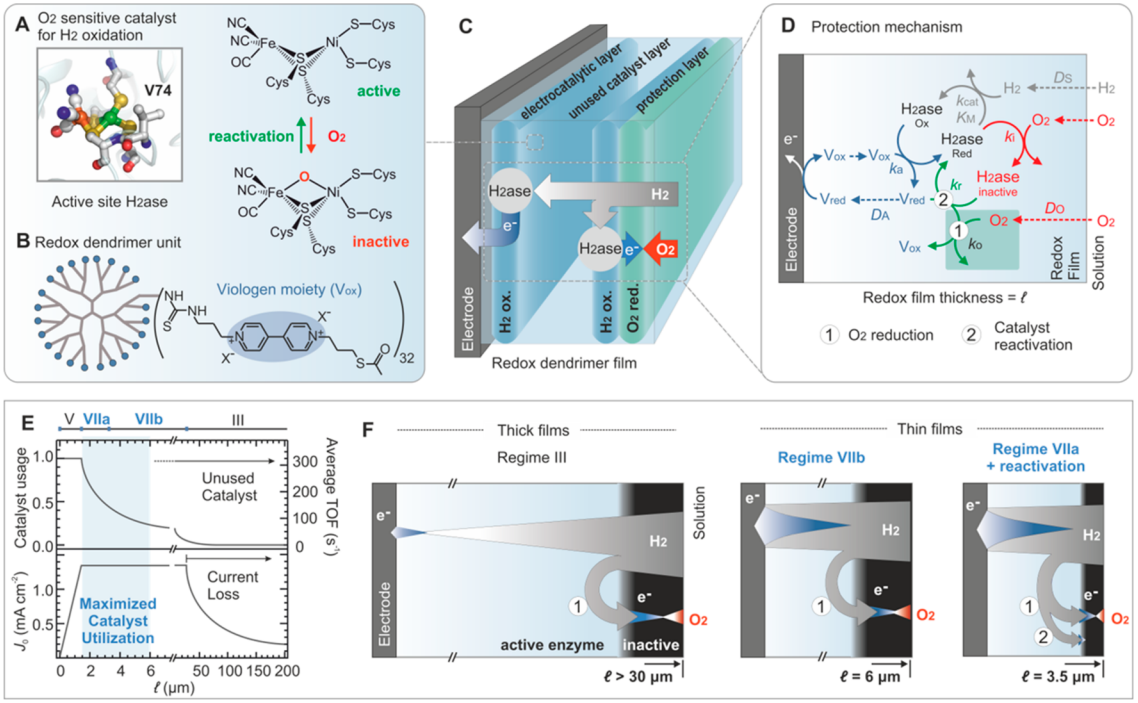


**Figure 1.** Redox films as protection matrices for hydrogenases. (A) Structure of the $[NiFe(CN)_2CN]$ active site of *D. fructosovorans* NiFe hydrogenase, used herein as a model of $O_2$-sensitive catalyst, showing the nearby valine 74 and its deactivation/reactivation in the presence of $O_2$. The whole enzyme is globular, with a diameter of ~10 nm, $M_w$ = 90 kDa. (B) Schematic representation of viologen-modified dendrimers (detailed structure is given in ref 20, diameter around 5 nm, $M_w$ = 20 kDa) used as building blocks for the assembly of the redox matrix. The viologen moieties act as electron relays and $O_2$-reducing catalysts. The thioacetate group is used as a cross-linking functionality for gelation, leading to film formation. (C) Scheme of the redox matrix homogeneously constituted of hydrogenase molecules and viologen-modified dendrimers. Under turnover for $H_2$ oxidation in the presence of $O_2$, several reaction layers form within the matrix. A first layer of $H_2$ oxidation reaction ($H_2$ ox.) in the vicinity of the electrode produces electrons used for current generation (electrocatalytic layer). A second $H_2$ ox. layer associated with a layer of $O_2$ reduction reaction ($O_2$ red.) near the film/electrolyte interface reduces the incoming $O_2$ (protection layer). (D) Kinetic scheme of the reaction–diffusion processes considered for modeling of the two proposed protection mechanisms: (1) reduction of the incoming $O_2$ and (2) reactivation of the inhibited catalyst. (Definitions of all parameters are given in Table S1.) (E) Fraction of the catalyst contributing to current (top) and catalytic current (bottom) under anaerobic conditions as a function of the film thickness. Regimes V, VII, and III are defined by Bartlett and Pratt[22] as cases in which the current is primarily limited by catalysis, electron transfer, and mass transport, respectively. VIIa and VIIb are the subregimes specific to protection from $O_2$ described in this Article. (F) Depiction of the fluxes of $H_2$ (gray), $O_2$ (red), and electrons (blue) associated with electrocatalysis and protection from $O_2$ in each of the different operating regimes (III, VIIb, and VIIa).

mediocre properties in terms of catalyst usage within the matrix and absolute current output.

Until now, thin films have not been explored in this context because thickness was assumed to be an inherent requirement for protection. In addition, the preparation of thin films embedding hydrogenase was impossible until recently because of the poor control of matrix morphology.

Here we apply a new method based on redox dendrimers that enables the formation of catalytic films of controlled and homogeneous thickness. Our results demonstrate not only that the robust $O_2$ protection of a catalyst in a film 6 $\mu$m thick is feasible but also that the observed catalytic protection is actually superior to that provided by analogous thick films. This protection coincides with the maximum performance in terms of the catalytic current (Figure 1F) while maintaining the stability and effective catalyst utilization required for technological applicability. We also show that the minimal thickness that affords $O_2$ immunity can be further decreased by using modified hydrogenases whose rate of reductive reactivation is increased. Under these conditions, the fraction of sacrificial catalyst is negligible. Theoretical models of the protection mechanisms that predict currents and concentration gradients within the redox matrix explain our empirical observation of the effectiveness of thin redox films against catalyst inactivation by $O_2$ and indicate that quasi-infinite protection can be achieved for the hydrogenase even when it is used in minimized loading. These are the key requirements for cost-effective and practical implementations of cheap molecular and bioinspired catalysts under the harsh oxidative conditions of energy-converting devices.

## RESULTS

Bioanodes utilizing *Desulfovibrio fructosovorans* NiFe hydrogenase as a catalyst in viologen-modified dendrimer films[20] of distinct thicknesses (66, 6, and 3.5 $\mu$m) were generated (see SI Section S2) to determine the enzyme stability and performance (Figure 2). For comparison, wild-type (WT, i.e., unmodified) NiFe hydrogenase and a previously described $O_2$-resistant V74C mutant[16] were cast in thin films. Whereas an $O_2$-sensitive NiFe hydrogenase directly connected to an electrode quickly becomes completely inactivated in the presence of $O_2$,[21] the same enzyme incorporated in a redox matrix is protected from $O_2$ damage,[10] as shown in Figure 2A. However, Figure 2 shows that the variation in $H_2$ oxidation catalytic current upon exposure to $O_2$ strongly depends on the film thickness and on the nature of the catalyst. Whereas the


DOI: 10.1021/jacs.9b06790
J. Am. Chem. Soc. 2019, 141, 16734–16742

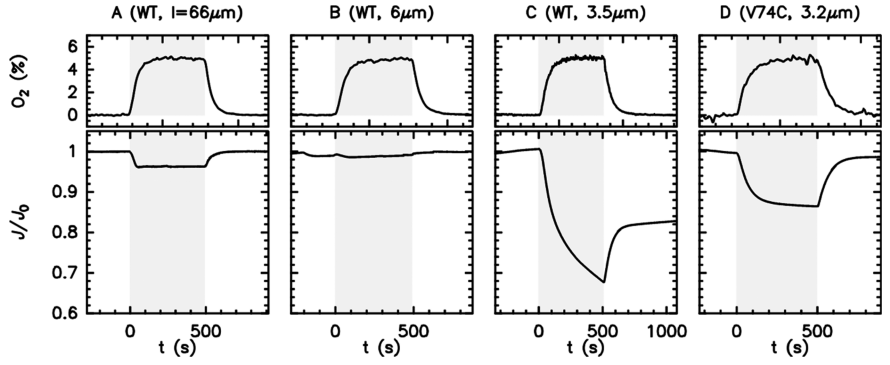


**Figure 2.** Experimental current responses of viologen-modified films embedding *Desulfovibrio fructosovorans* NiFe hydrogenase, catalyzing $H_2$ oxidation, and being exposed to $O_2$. Wild-type (WT, i.e., unmodified) NiFe hydrogenase embedded in films with decreasing thicknesses from left to right: (A) 66 $\mu$m, regime III; (B) 6 $\mu$m, regime VIIb; and (C) 3.5 $\mu$m, regime VIIa. (D) $O_2$-resistant site-directed mutant (V74C[16]) embedded in a film with a thickness corresponding to regime VIIa for comparison with panel C. The behavior of films in regimes III and VIIb using the V74C mutant is shown in Figure S1. The top panels show the $O_2$ concentration (the shaded areas represent $O_2$ exposure), and the bottom panels show the change in $H_2$ oxidation current divided by the value under anaerobic conditions, $J/J_0$, against time, $t$, counted from the beginning of exposure to $O_2$. The anaerobic conditions correspond to 100% $H_2$. Aerobic conditions correspond to 5% $O_2$ in 95% $H_2$. Note that 5% $O_2$ is just below the explosion limit for $H_2/O_2$ gas mixtures[17] and well above what would be expected under operational conditions in a fuel cell. In all cases, iodide was present in the electrolyte (phosphate buffer, 0.1 M, pH 7 with KI 0.1 M) to minimize $H_2O_2$ accumulation;[18,19] this is more convenient than including large enzymes such as catalase. The electrodes were held at a constant potential of 0.21 V versus SHE and rotated at 2000 rpm. The current behavior of films with thicknesses near the regime transitions (4.5 and 33 $\mu$m) is shown in Figure S2.

thickest film (66 $\mu$m) shows a loss in current that is fully reversed by the removal of $O_2$ (Figure 2A), films that are one order of magnitude thinner (6 $\mu$m) are apparently completely unaffected by $O_2$ (Figure 2B). With a film that is only slightly thinner (3.5 $\mu$m), the catalytic current rapidly collapses and is only partially recovered upon returning to anaerobic conditions (Figure 2C). In contrast, when the V74C $H_2$ase mutant is used, the aerobic current of this thinnest film drops to a steady-state value and fully recovers after $O_2$ is removed (Figure 2D).

We used theoretical modeling (Figures 3–6) to explain these unexpected experimental observations and elucidate the underlying kinetics in the reaction–diffusion systems (Figure 1D). We have considered the diffusion and reaction of the various species (reduced and oxidized viologen; reduced, oxidized, and inactive enzyme; $O_2$ and $H_2$) within the depth of the film, the thickness of which is $l$. We also considered the diffusion of substrate $H_2$ and $O_2$ (diffusion coefficients $D_S$ and $D_O$, respectively) and electron hopping between the immobilized viologen moieties. (This is also a diffusion process, with an apparent diffusion coefficient of the electron $D_A$; $A^\Sigma$ is the viologen concentration.) The enzyme (total concentration $E^\Sigma$) is immobilized and reacts with the oxidized viologen (rate constant $k_a$) and with the substrate $H_2$ (Michaelis parameters $k_{cat}$, $K_M$); it can also be inactivated by $O_2$ (bimolecular inactivation rate constant $k_i$) and reactivated upon the reaction with reduced viologen (bimolecular rate constant $k_r$). The reduced viologen also reduces $O_2$ with a bimolecular rate constant $k_o$.[11] The reaction–diffusion system depends on 16 independent parameters (three diffusion coefficient, four concentrations, seven kinetic parameters, film thickness, and time). Figures 3–6 and Figure S1 show numerical solutions of the model obtained by varying only two parameters (the thickness of the film and the rate, $k_r$, at which the inactive enzyme is reactivated upon reduction); all other parameters were fixed to their experimentally determined values. (See the details in SI Sections S3 and S4).

To frame the various rates of diffusion, kinetic reactions, and protective states within the films, we discuss our results in terms of different "regimes", each of which defines a region of the parameter space for which the system behaves in a certain manner. Bartlett and Pratt[22] defined seven regimes for the case of a uniform film containing a mediator and an enzyme under anaerobic conditions. For example, the so-called "regime III" (described for the anaerobic conditions in ref 22 and for the aerobic conditions in ref 11), is observed when the dimensionless thickness of the film $\kappa = l\sqrt{k_a E^\Sigma / D_A}$ is large; it corresponds to the situation of very thick films, where the current response is limited by the long-range diffusion of the substrate and electrons, as described before.[11] In SI Section S5, we demonstrate the kinetic regime assignments before $O_2$ exposure.

**Thick Films (Regime III, Figures 2A and 3).** For the sake of comparison with our new results, we start by recalling the experimental behavior[10] and theory[11] for a thick viologen-modified film containing hydrogenase.[22] In thick films, the oxidation of $H_2$ is confined to a region close to the electrode where the concentration profiles of oxidized viologen and hydrogen overlap. (The peak in gray in the top panel of Figure 3A shows where $H_2$ is consumed.) The resulting steady-state catalytic anaerobic current density $J_0$ is limited by the mass transport of both $H_2$ and electrons; the thicker the film, the stronger the limitations due to mass transport, and the smaller the current

$$\frac{J_0}{F} = \frac{D_S S^\infty + D_A A^\Sigma}{l} \approx \frac{D_S S^\infty}{l} \quad (1)$$

The anaerobic current is essentially proportional to the bulk concentration of $H_2$ ($= S^\infty$), as indeed experimentally observed for the 66 $\mu$m film (Figure S6A). According to the parameter values in SI Section S3, films thicker than 29.5 $\mu$m are in regime III. This is confirmed by the experimental current response to $O_2$ of a film with a thickness just above this regime transition (33 $\mu$m, Figure S2B), which displays similar behavior to the 66 $\mu$m thick films. Moreover, for films with $l$ > 29.5 $\mu$m, the experimental anaerobic current density decreases with increasing film thicknesses (0.62 ± 0.06 mA/cm$^2$ for $l \approx$ 30


DOI: 10.1021/jacs.9b06790
J. Am. Chem. Soc. 2019, 141, 16734–16742

$\mu$m compared with 0.38 ± 0.1 mA/cm$^2$ for $l \approx 60$ $\mu$m), which is in agreement with eq 1 and thus further supports the regime III assignment.

Introducing $O_2$ into the solution slightly decreases the steady-state catalytic current density, $J$, as observed in Figure 2A (66 $\mu$m film) and previously predicted[11]

$$\frac{J}{J_0} = \frac{D_S S^\infty - D_O O^\infty}{D_S S^\infty + D_A A^\Sigma} \quad (2)$$

The numerical application of eq 2 based on the parameter values listed in Table S1 gives $J/J_0 = 0.96$, in agreement with the experimental results in Figure 2A and Figure S2 and the simulation in Figure 3D. Regarding the transient response and the results from the model given in Figure 3 (and also Figures 4−6 and Figure S1), the only significant difference between the experimental and simulated currents is that the former shows a gradual current change, whereas the latter show a sharp step upon the addition of $O_2$. This is because we simulate the current for an instantaneous change in $O_2$ concentration, whereas the experimental current reacts to a gradual change in $O_2$ concentration (controlled by purging the electrolyte with a gas mixture containing 5% $O_2$). The transient in the current follows the experimental change in $O_2$ concentration given in the top panels of Figure 2.

The protection mechanism can be understood by examining the corresponding concentration profiles (Figure 3B).[11] Dioxygen (whose concentration profile is shown in red) penetrates the film, inactivates the enzyme, and oxidizes the viologen near the film/solution interface. The oxidized viologen (pink) diffuses inward, allowing catalytic hydrogen oxidation in an outer catalytic layer (peak at $\xi = 0.93$ in Figure 3B, top panel). The resulting reduced viologen (blue) diffuses out and consumes the incoming $O_2$ in the outermost reaction layer (red peak at $\xi = 0.97$ in Figure 3B). Exposing the film to $O_2$ decreases the hydrogen oxidation current because $O_2$ reduction uses a fraction of the incoming flux of $H_2$. The enzyme is inactivated by $O_2$ in an outer layer comprised between $x = x_f$ and $x = l$, where $l$ is the thickness of the film. The size $l - x_f$ of this layer of inactive enzyme (black in Figure 3B) keeps increasing, very slowly, in proportion to the logarithm of time[11] (eq 3)

$$\frac{d(l - x_f)}{d \ln t} \approx \frac{3 D_O^{3/2} O^\infty}{2 k_o^{1/2} D_A A^{\Sigma\,3/2}} \quad (3)$$

The dashed red line in Figure 3D shows this prediction. The only difference from Fourmond et al.[11] is that we better estimated the duration of the transient (that is, the time delay between the exposure to $O_2$ and the moment the front of the inactive enzyme starts moving in at a steady-state rate, $\log_{10}(\tau) = 1.2$ in Figure 3D; see SI Section S6.4 and eqs S6.62 and S6.70). This transient ($\log_{10}(\tau) < 1$) corresponds to the initial penetration of $O_2$, followed by the inactivation of the enzyme in this outer region of the film; the latter step is the slowest (with the values of the parameters in Table S1) and fully determines the duration of the transient, which is therefore proportional to the reciprocal of $k_i$. The rate of progression of the front of inactive enzyme (eq 3 and red line in Figure 3D) does not depend on $k_i$, but the duration of the transient (eq S6.70), and therefore the lifetime of the film (eq S6.73), depends on $k_i$. However, eq S6.73 shows that the parameters present in eq 3 (which are all independent of the properties of the catalyst) have a much bigger impact on the lifetime than $k_i$. We also note that despite the movement of the front of inactive enzyme, the aerobic current is constant (eq 2).[11]

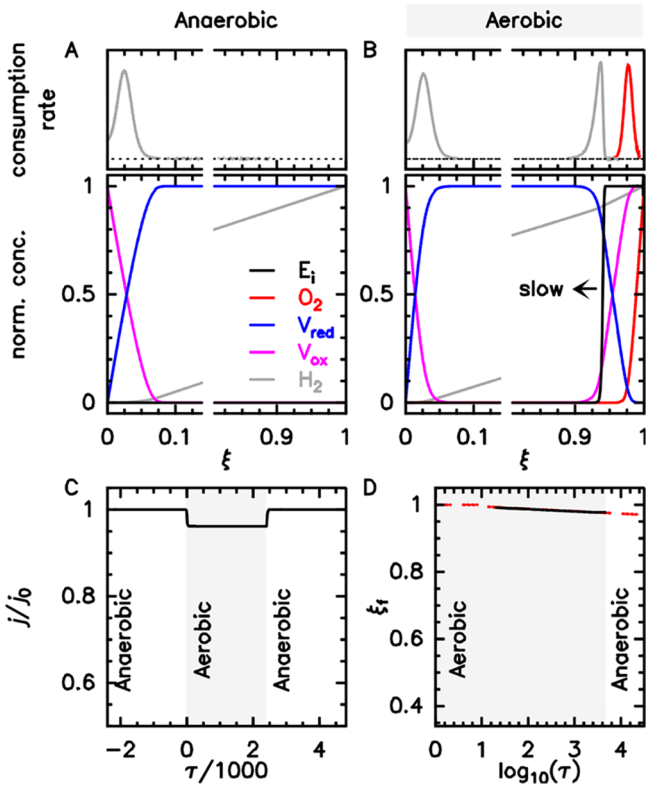


**Figure 3.** Simulated concentration profiles within the thick film (66 $\mu$m, regime III) explaining the current response shown in Figure 2A and predicting the protection lifetime. (A) Anaerobic and (B) aerobic dimensionless calculated concentration profiles within the viologen-modified films embedding WT hydrogenase, catalyzing $H_2$ oxidation (bottom panels). The black arrow illustrates the rate of progress of the front of the inactive enzyme. A discontinuous $x$ axis is used to zoom in on the thin reaction layers near the inner and outer edges of the film. The local rates of consumption (top panels) of $H_2$ (gray) and $O_2$ (red) are obtained from the second derivative of the concentration profile of each species; the horizontal dotted lines mark $Y = 0$. The dimensionless distance to the electrode $\xi$ is $x/l$. (C) Change in simulated current divided by the value under anaerobic conditions, $j/j_0$, against dimensionless time, $\tau$ ($\tau = tk_aE^\Sigma$, counted from the beginning of exposure to $O_2$). (D) Simulated position of the front of the inactive enzyme, $\xi_f$, against dimensionless time; the dashed red line is the model. (See SI Section S6.4 and eqs S6.62 and S6.70).

Most importantly, the protection of thick films in regime III results from the separation of reaction zones (Figure 3B, top panel) and from the very slow movement of the invading layer of inactive enzyme, which together provide very long lifetimes. This protection comes at a cost: Most of the catalyst is unused or used for protection rather than catalysis (Figure 1F), and the current is limited by long-range diffusion.

**Thin Films in Regime VII under Anaerobic Conditions (Figures 2B,C, 4, and 5).** The 6 and 3.5 $\mu$m films are in what Bartlett and Pratt referred to as regime VII.[22] Under anaerobic conditions, the concentration profiles are as shown in Figures 4A and 5A (bottom panels): There is little $H_2$ depletion in the film, and the current is limited by the rate of electron transfer. $H_2$ oxidation occurs near the surface of electrode in a steady-state reaction layer whose size is determined by the mutual



DOI: 10.1021/jacs.9b06790
J. Am. Chem. Soc. 2019, 141, 16734−16742

compensation of $H_2$ oxidation and electron diffusion, and the anaerobic current is therefore independent of $l$[22]

$$J_0 = F\sqrt{\frac{2D_A A^{\Sigma} k_{cat} E^{\Sigma}}{1 + K_M/S^{\infty}}} \quad (4)$$

Figure S6B,C confirms for the 6 and 3.5 $\mu$m films the nonlinear dependence of the value of the current on the $H_2$ concentration under anaerobic conditions, in quantitative agreement with eq 4. The experimental value for the anaerobic current density in regime VII is 0.55 ± 0.1 mA/cm$^2$ (for the four electrodes in regime VII shown in Figure 2 and Figure S2).

In considering the additional effect of $O_2$, we shall distinguish two subcases of regime VII, VIIb (Figure 4, 6 $\mu$m) and VIIa (Figure 5, 3.5 $\mu$m).

**Thin Films under Aerobic Conditions (Regime VIIb, Figures 2B and 4).** Unexpectedly, we found that decreasing the film thickness does not come at the expense of resistance to $O_2$. Exposure to $O_2$ actually has no effect on the current of the 6 $\mu$m thick film (Figure 2B), consistent with the corresponding simulation in Figure 4C. The aerobic concentration profiles in Figure 4B (bottom panel) explain why the current is nearly independent of the presence of $O_2$: As in regime III, the reduction of $O_2$ decreases the incoming flux of $H_2$ and the concentration of $H_2$ in the inner reaction layer, but because the concentration of $H_2$ remains greater than the Michaelis constant, the enzyme remains saturated. Therefore, the decrease in $H_2$ concentration has little impact on the catalytic rates and thus on the current.

In SI Section S6.3.1, we demonstrate that the relative change in current upon exposure to $O_2$ in regime VIIb is

$$\frac{J}{J_0} = 1 - \frac{D_A A^{\Sigma}}{2D_S S^{\infty}(1 + S^{\infty}/K_M)} \quad (5)$$

The observed decrease in current is actually tiny because the $K_M$ of NiFe hydrogenase is small (~5 $\mu$M, ref 21). The above estimation assumes that under anaerobic conditions, there is no depletion of $H_2$; numerical application gives $1 - J/J_0 = 7 \times 10^{-5}$ compared with $7 \times 10^{-4}$ in Figure 4C. A more accurate estimation, taking the depletion of $H_2$ into account and giving $1 - J/J_0 = 1.1 \times 10^{-4}$, is described in SI Section S6.3.1. Note that eq 5 is independent of the bulk concentration of $O_2$.

In this regime, although the current is not significantly affected by the presence of $O_2$, the layer of inactive enzyme keeps moving in, as shown in Figure 4D, where the dashed line shows the theoretical prediction: The rate of progression is the same as in regime III (eq 3). Supplementary Figure S12 shows a plot of simulated and calculated lifetimes versus $l$ for the conditions in Figure 4. Under the conditions of Figure 2B, we calculate that the film becomes totally invaded with an inactive enzyme at $\tau = 10^{8.2}$, corresponding to 1 year (with $\tau/t = k_a E^{\Sigma} = 4.8$; see Figure S11). More generally, increasing the film thickness by 1 $\mu$m increases the lifetime by over two orders of magnitude (Figure S12). From a practical perspective, this means that the hydrogenase in the electrocatalytic reaction layer can be protected quasi-infinitely from $O_2$ in this regime.

**Even Thinner Films under Aerobic Conditions (Regime VIIa, Figures 2C and 5).** The independence of the catalytic hydrogen oxidation current on $O_2$ observed in Figure 2B results from the separation of the two $H_2$ oxidation reaction layers (Figure 4B, top panel). A distinct subclass of

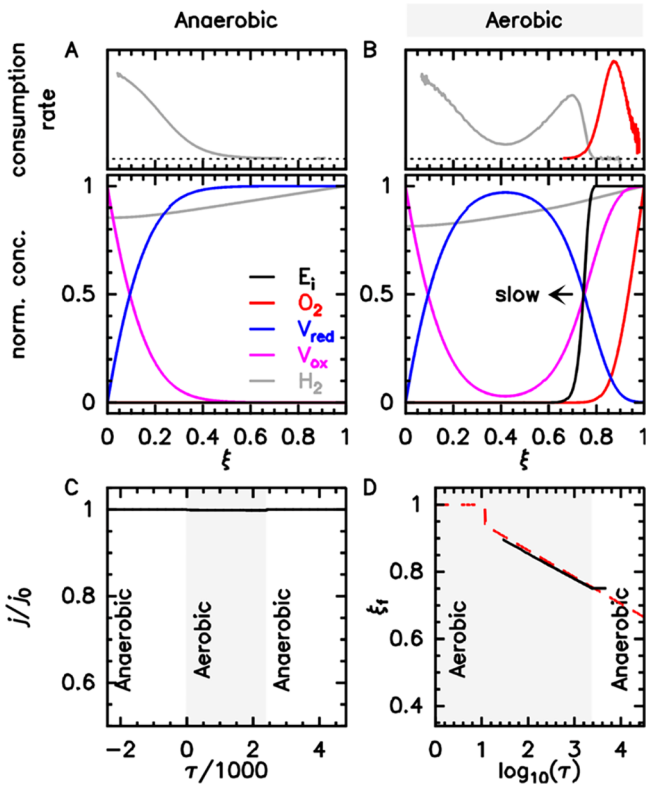


**Figure 4.** Simulated concentration profiles within the thin film (6 $\mu$m, regime VIIb) explaining the current response shown in Figure 2B and predicting the protection lifetime. (A) Anaerobic and (B) aerobic dimensionless calculated concentration profiles within the viologen-modified films embedding WT hydrogenase, catalyzing $H_2$ oxidation (bottom panels). The black arrow illustrates the rate of progress of the front of the inactive enzyme. The local rate of consumption of $H_2$ (gray) and $O_2$ (red) was obtained from the second derivative of the concentration profile of each species (top panels). (C) Change in simulated current divided by the value under anaerobic conditions, $j/j_0$, against $\tau$. (D) Simulated position of the front of the inactive enzyme $\xi_f = x_f/l$ against dimensionless time, $\tau$ ($O_2$ is introduced at $\tau$ = 0); the dashed red line is the model. (See SI Section S6.4 and eqs S6.62 and S6.70). See SI Section S7 and Figure S11 for the result of a simulation of constant exposure to $O_2$ until the film collapses.

regime VII (that we call VIIa) is observed when the film is so small that the two $H_2$ oxidation catalytic layers merge, as shown in Figure 2C with a film of 3.5 $\mu$m. This film is still in regime VII under anaerobic conditions, so the equation for the anaerobic current is as described above (eq 3), but the relative decrease in current just after the film is exposed to $O_2$ is significant, as explained in SI Section S6.2. The formation of a single $H_2$ oxidation catalytic layer implies that current generation and protection from $O_2$ compete for electrons, which significantly decreases the reduced viologen concentration gradients (Figure 5B). Hence the flux of electrons toward the film−electrolyte interface decreases to the extent that it does not counterbalance the flux of $O_2$. The imbalance is amplified by the formation of an inactive enzyme, which leads to fast $O_2$ penetration in the very thin film (Figure 5B, bottom panel, and Figure 5D), and, indeed, a simulation such as that in Figure 5D but with continuous exposure to $O_2$ predicts a short lifetime of ~10 min.

The two $H_2$ oxidation reaction layers in Figure 4B (top panel) have the same size, equal to the size of the unique reaction layer under anaerobic conditions (Figure 4A, top


DOI: 10.1021/jacs.9b06790
J. Am. Chem. Soc. 2019, 141, 16734−16742

panel). Therefore, the transition between the thicker and thinner regime VII occurs for a film thickness that is twice that of the anaerobic reaction layer (eq 6 and eq S6.44)

$$l = \left(2 + \frac{D_O O^\infty}{2 \times D_A A^\Sigma}\right)\sqrt{\frac{2D_A A^\Sigma\left(1 + \frac{K_M}{S^\infty}\right)}{k_{cat}E^\Sigma}} \quad (6)$$

Numerical application using the parameter values in Table S1 gives $l$ = 3.25 $\mu$m for the transition between regimes VIIa and VIIb. This value is just below the thickness of the film of Figure 2C, suggesting that the latter is actually in regime VIIb; however, the progression of $O_2$ inside the film rapidly makes the two catalytic regions collapse so that the profiles in Figure 5B are compatible with the "thinnest films" behavior in which protection is not sustained (VIIa), as indeed demonstrated by the fast decay of the catalytic current observed upon exposure to $O_2$ (Figure 2C). For comparison, a slightly thicker film (4.5 $\mu$m, Figure S2A), shows a clear regime VIIb behavior (experimental catalytic current unaffected by $O_2$), which supports the value of 3.25 $\mu$m as the transition between regimes VIIa and VIIb.

**Additional Protection Mechanism Operational in the Thinnest Films (VIIa, Figures 2D and 6).** The inactivation of NiFe hydrogenase by $O_2$ is mostly reversible: It leads to a mixture of inactive states that can be reactivated by reduction.[23] However, the reaction with $O_2$ is strongly dependent on the side chain of the position 74 residue (Figure 1A),[24,25] and, in particular, replacing valine 74 with cysteine accelerates the reactivation of the oxidized enzyme.[16,24,26] Here we observe that the V74C mutation abolishes the $O_2$ sensitivity in the very thin hydrogenase film: Figure 2D shows that the current obtained with a very thin film (3.2 $\mu$m) incorporating the V74C hydrogenase mutant reaches a steady-state value under 5% $O_2$ instead of quickly decreasing, as observed for the WT enzyme in Figure 2C.

The experimental behavior is simply accounted for by the model by a single change: setting a nonzero value of the rate of reactivation of the enzyme by the reduced viologen (whereas $k_r$ = 0 in the simulations in Figures 3–5, all other parameters being the same). This reaction is indicated by the label (2) in Figures 1D and 1F. The concentration profiles in Figure 6B reach a true steady state, implying that the protection can theoretically be effective forever (compared with a stability of minutes for the corresponding film incorporating the WT enzyme, Figure 2C). Stabilization is possible because as the front of the inactive enzyme moves in, the concentration of $O_2$ at the front decreases, whereas the concentration of the reduced mediator remains the same. Thus there is an $O_2$ penetration depth for which the inactivation of active enzymes by $O_2$ is exactly balanced by the reactivation of inactive enzymes.

Figure 6E shows the position of the stationary front of an inactive enzyme, $\xi_f$, as a function of the ratio of the rate constants of reactivation over inactivation for various values of the film thickness (all in dimensionless forms; see SI Section S6.5). The greater the $k_r/k_i$, the smaller the $O_2$ penetration depth ($\xi_f$ is closer to 1). Increasing the film thickness ($\kappa$) decreases the value of $k_r/k_i$ that is necessary to stabilize a certain value of $\xi_f$. The exact value of $\kappa$ matters very much: Increasing $\kappa$ from 5.5 to 7.5, that is, <30%, decreases the value of $k_r/k_i$ that stabilizes a given $\xi_f$ (here $\xi_f$ = 0.6, horizontal gray dashed line in Figure 6E) by more than two orders of magnitude. The curves in Figure 6E all end vertically below a certain value of $k_r/k_i$, which strongly depends on the film thickness: This is the minimum value of $k_r/k_i$ that affords long-lasting protection. Figure 6F shows the steady-state value of $j/j_0$ corresponding to the penetration depth of Figure 6E. It increases with both $\kappa$ and $k_r/k_i$; if $k_r/k_i$, is large enough that the film is protected, then the steady-state current is nearly independent of $k_r/k_i$. The black circle in Figure 6E marks the value predicted for the experiment shown in Figure 2D. Note the close agreement between the exact value of $j/j_0$ (0.86 in Figures 6C) and the value approximated here (0.965, marked by a dot in Figure 6F).

Control experiments where we embedded the V74C mutant in thicker films are shown in Figure S1. In regimes VIIb and III, the current responses for the wild-type hydrogenase and V74C mutant are identical (Figures 2A,B and Figure S1, respectively). This confirms that the protection is primarily defined by the $O_2$ reduction reaction catalyzed by the viologen in these regimes. Nevertheless, the faster reactivation rate of V74C leads to a steady-state position of the front of the inactive enzyme (Figure S1, row 7) because a balance between

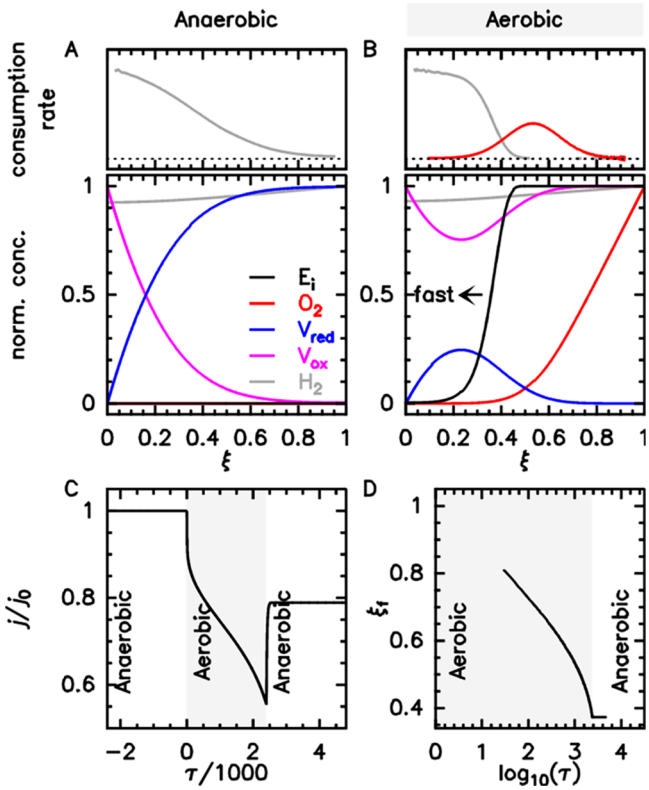


**Figure 5.** Simulated concentration profiles within the thinnest film (3.5 $\mu$m, regime VIIa) explaining the current response shown in Figure 2C and predicting the protection lifetime. (A) Anaerobic and (B) aerobic dimensionless calculated concentration profiles within the viologen-modified films embedding WT hydrogenase, catalyzing $H_2$ oxidation (bottom panels). The black arrow illustrates the rate of progress of the front of the inactive enzyme. The local rate of consumption of $H_2$ (gray) and $O_2$ (red) was obtained from the second derivative of the concentration profile of each species (top panels); the horizontal dotted lines mark $Y$ = 0. The dimensionless distance to the electrode $\xi$ is $x/l$. (C) Change in the simulated current divided by the value under anaerobic conditions, $j/j_0$, against $\tau$. (D) Simulated position of the front of the inactive enzyme, $\xi_f$, against dimensionless time, $\tau$.



DOI: 10.1021/jacs.9b06790
J. Am. Chem. Soc. 2019, 141, 16734–16742

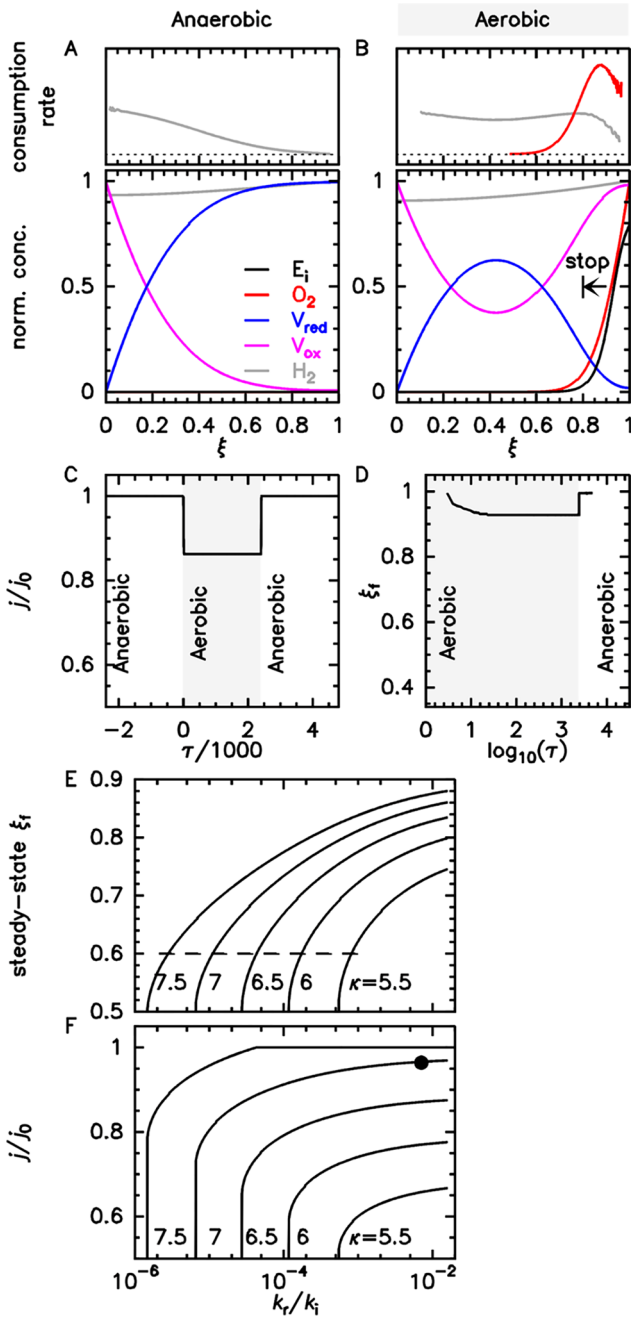


**Figure 6.** Effect of the reactivation of the enzyme by reduced viologen on the behavior of the thin film in regime VIIa, as observed in Figure 2D. (A) Anaerobic and (B) aerobic dimensionless simulated concentration profiles within the viologen-modified films embedding $O_2$-resistant site-directed mutant (V74C) hydrogenase, catalyzing $H_2$ oxidation (bottom panels). The black arrow illustrates the rate of progress of the front of the inactive enzyme. The local rate of consumption of $H_2$ (gray) and $O_2$ (red) was obtained from the second derivative of the concentration profile of each species (top panels); the horizontal dotted lines mark $Y = 0$. The dimensionless distance to the electrode $\xi$ is $x/l$. (C) Change in simulated current divided by the value under anaerobic conditions, $j/j_0$, against $\tau$. (D) Simulated position of the front of the inactive enzyme $\xi_f$ against dimensionless time $\tau$. (E) Dependence of the normalized position of the front of the inactive enzyme, $\xi_f$, and (F) the aerobic current, $j/j_0$, as a function of the dimensionless rate of reactivation $k_r/k_i$ for various values of the dimensionless thickness, $\kappa$; see SI Section S6.5. The black dot indicates the situation in Figure 2D. Calculations were for the values of the parameters in Table S2.

reactivation and deactivation is reached, like for the thin films of V74C hydrogenase in regime VIIa (Figure 2D).

## DISCUSSION

The experimental and theoretical data presented here describe a novel protection regime for $O_2$-sensitive catalysts in thin films (<6 $\mu$m) consisting of cross-linked viologen-modified dendrimers. It was previously reported that protection could occur only in thick films (>100 $\mu$m) in which only a tiny fraction of the catalyst (e.g., ~0.3% for a thickness of 100 $\mu$m, Figure 1E) contributed to the current generation. Here we demonstrate that not only are $O_2$-sensitive catalysts protected from damage in thin redox films with a thickness of just 6 $\mu$m, but also, remarkably, the protection is even more robust than that reported for thick films. Indeed, in thick films (regime III), the current drops significantly after exposure to $O_2$ (Figure 2A). In thin films (VIIb), the catalytic current is virtually unaffected by the exposure to $O_2$, and the protection remains long-lasting (Figures 2B and 4). Thinner films (3.5 $\mu$m, regime VIIa) do not resist $O_2$ (Figures 2C and 5) unless an additional protection mechanism is operational to provide long-term protection (Figures 2D and 6).

The change in catalytic current over time (or the absence thereof) when the hydrogenase/polymer film is exposed to $O_2$ (Figure 2) reveals the extent of the protection in each case considered, but the underlying protection mechanism cannot be deduced from the electrochemical response alone. Therefore, we used a reaction diffusion model to predict the time-resolved concentration gradients and positions of the catalytic layers inside the film; the behavior of the system depends on the values of parameters that could all be independently determined. The model succeeds in predicting the dependence of current on the $O_2$ and $H_2$ concentration as well as the transition between the two newly identified regimes, namely, VIIa and VIIb.

Despite different current responses between regimes III and VIIb, the protection can be explained by the exact same mechanism involving the viologen-catalyzed $O_2$ reduction close to the outer film boundary, which balances the inward flux of $O_2$. The condition for efficient protection is that the two catalytic layers for $H_2$ oxidation remain spatially separated to avoid any competition for electrons between the process for current generation and the process for protection. The reason for the peculiar behavior in regime VIIb (the absence of the effect of $O_2$ on the current) is that in thin films the concentration of $H_2$ remains well above the Michaelis constant, even if it is slightly depleted as a result of $O_2$ consumption. The lifetime of the film is defined by two contributions, namely, the initial rate of enzyme deactivation at the film/solution interface just after the exposure to $O_2$ and the rate of the subsequent progression of the front of the inactive enzyme within the film. Whereas the duration of the former depends on the kinetic constant for catalyst inactivation, $k_i$ (eq S6.70), the latter depends only on the parameters that define the film properties (eq 3). In particular, the lifetime of the film strongly depends on the viologen concentration and the apparent diffusion coefficient of the electron ($A^{\Sigma}$ and $D_A$). With the system made of viologen dendrimers described herein, the value of the product $D_A A^{\Sigma 3/2}$, which defines the progress of the front of the inactive enzyme (eq 3), is about five times larger than that for the previously reported redox matrices.[11] Equation 3 and Equation S6.73 also show that the lifetime of the film scales


DOI: 10.1021/jacs.9b06790
J. Am. Chem. Soc. 2019, 141, 16734−16742

exponentially with its thickness. The model predicts that the lifetime of a 6 $\mu$m film made of these viologen-modified dendrimers is 1 year (Figures S11 and S12); a further increase in film thickness by just 2 $\mu$m theoretically leads to a lifetime of 22 000 years. These values are well beyond the intrinsic anaerobic stability of hydrogenase, with a half life of 6 weeks,[10] or of the matrix itself, whose lifetime is limited by the $H_2O_2$ generation that degrades the viologen moieties.[27]

Importantly, although the film lifetime is proportional to the reciprocal of the rate constant of the inactivation of the catalyst by $O_2$ ($k_i$), this effect can easily be compensated by adjusting the film parameters because the latter contribute to the exponential component defining the lifetime in eq S6.73. For instance, an eight order of magnitude increase in inactivation rate can be compensated by just a 4 $\mu$m increase in film thickness.

Overall, the very thin films are particularly advantageous because the fraction of catalyst contributing to current is enhanced by two orders of magnitude (up to half of the catalyst load in regime VIIb), the current output is maximal (owing to fast mass transport of $H_2$) and immune to $O_2$, and the lifetime remains well above that required for real-world applications.

The minimal thickness that affords long-term protection according to the mechanism described above defines the boundary between regimes VIIa and VIIb, where the two catalytic layers for $H_2$ oxidation merge (eq 6), but we also demonstrated that the redox matrix can be used to induce reactivation, which leads to the prediction of everlasting protection, even in the thinnest films (3.2 $\mu$m thick, regimes VIIa). The reductive reactivation of hydrogenase occurs for hydrogenases either undergoing direct electron transfer with electrodes[24,28,29] or interfaced by redox films,[15,30] but these previous reports suggested that the electrons needed for reactivation originated from the electrode. Such protection was effective only at a low electrode potential[15] because the rate of reactivation decreases exponentially as the electrode potential increases.[29] High electrode potentials, which do occur in fuel cells under anode-limiting conditions, resulted in complete and irreversible fuel cell shutdown even when using the most resistant hydrogenases.[31] In contrast, we demonstrate here that in the redox-active films the electrons used for reactivation are exclusively generated from the $H_2$ oxidation catalyzed by an active hydrogenase in the vicinity of the layer of the inactive enzyme. This matrix-triggered reactivation is analogous to biological pathways that enable the reactivation of hydrogenase through their neighbors via electron transfer.[32,33] With a mechanism that is independent of the electrode as an electron source, reactivation becomes possible regardless of the operating conditions of the fuel cell and thus serves as a built-in safeguard against uncontrolled oxidative shutdown. Films operating in regime VIIb and embedding enzymes that can reductively reactivate are particularly advantageous because the protection from $O_2$ theoretically lasts forever and the anaerobic currents are fully immune to $O_2$.

## CONCLUSIONS

We experimentally demonstrated and theoretically elucidated the mechanism of protection of catalysts in redox films in the complete range of catalytic regimes related to the film thicknesses relevant for applications. Two major and unexpected findings could make the research community rethink catalyst use and design. First, micrometer-thick films are sufficient to efficiently protect fragile catalysts such as hydrogenase, enabling their use in energy-converting devices without compromising the current generation efficiency or immobilizing large amounts of unused catalyst. The only requirement is that the matrix efficiently diverts electrons from the catalysts for the reduction of $O_2$. Because even a large inactivation kinetic constant of the catalysts can be easily counterbalanced by minor changes in parameters defining the film properties (in particular, its thickness), highly $O_2$-sensitive catalysts can now be considered for applications without the need to decrease their inactivation rate. Second, the matrix can further enhance protection from $O_2$ for an infinite time period by using a fraction of the electrons diverted from $H_2$ oxidation (rather than from the electrode) to reactivate the catalyst and thus stop the progression of the layer of the inactive catalyst. This creates novel opportunities to utilize reactivation kinetics, even under the uncontrolled and oxidative conditions encountered in operating fuel cells. The quantitative description of the requirements in terms of the catalyst reactivation kinetics and the film properties presented here will guide the future development of biological or bioinspired catalysts that reductively reactivate, as indeed recently observed in synthetic mimics of the NiFe hydrogenase active site,[34] to achieve robust operation, even under the harsh oxidative conditions of $H_2/O_2$ fuel cells and other energy-converting devices.

## ASSOCIATED CONTENT

### Supporting Information

The Supporting Information is available free of charge on the ACS Publications website at DOI: 10.1021/jacs.9b06790.

Procedures, model and analytical solutions, Figures S1−S12, and Tables S1−S5 (PDF)

## AUTHOR INFORMATION


### Corresponding Authors

*E-mail: nicolas.plumere@rub.de.
*E-mail: vincent.fourmond@imm.cnrs.fr.
*E-mail: christophe.leger@imm.cnrs.fr.

### ORCID

Christophe Léger: 0000-0002-8871-6059
Vincent Fourmond: 0000-0001-9837-6214
Nicolas Plumeré: 0000-0002-5303-7865


### Notes

The authors declare no competing financial interest.

## ACKNOWLEDGMENTS

C.L., V.F., and S.D. are supported by CNRS, Aix Marseille Université, Agence Nationale de la Recherche (ANR-15-CE05-0020), and the Excellence Initiative of Aix-Marseille University - A*MIDEX, a French "Investissements d'Avenir" programme (ANR-11-IDEX-0001-02). N.P., D.B., and H.L. acknowledge financial support by RESOLV, funded by the Deutsche Forschungsgemeinschaft (DFG, German Research Foundation) under Germany's Excellence Strategy − EXC-2033 − Projektnummer 390677874, by the ERC starting grant 715900, and by the ANR-DFG project SHIELDS (PL 746/2-1). H.L. is grateful for the support by the China Scholarship Council (CSC). The French authors are part of FrenchBIC (www.frenchbic.cnrs.fr).



DOI: 10.1021/jacs.9b06790
J. Am. Chem. Soc. 2019, 141, 16734−16742

## REFERENCES


(1) Le Goff, A.; Artero, V.; Jousselme, B.; Tran, P. D.; Guillet, N.; Métayé, R.; Fihri, A.; Palacin, S.; Fontecave, M. From Hydrogenases to Noble Metal-Free Catalytic Nanomaterials for $H_2$ Production and Uptake. *Science* **2009**, *326* (5958), 1384−1387.

(2) Tran, P. D.; Le Goff, A.; Heidkamp, J.; Jousselme, B.; Guillet, N.; Palacin, S.; Dau, H.; Fontecave, M.; Artero, V. Noncovalent Modification of Carbon Nanotubes with Pyrene-Functionalized Nickel Complexes: Carbon Monoxide Tolerant Catalysts for Hydrogen Evolution and Uptake. *Angew. Chem., Int. Ed.* **2011**, *50* (6), 1371−1374.

(3) Artero, V.; Chavarot-Kerlidou, M.; Fontecave, M. Splitting Water with Cobalt. *Angew. Chem., Int. Ed.* **2011**, *50* (32), 7238−7266.

(4) Helm, M. L.; Stewart, M. P.; Bullock, R. M.; DuBois, M. R.; DuBois, D. L. A Synthetic Nickel Electrocatalyst with a Turnover Frequency above 100,000 $s^{-1}$ for $H_2$ Production. *Science* **2011**, *333* (6044), 863−866.

(5) Singh, W. M.; Baine, T.; Kudo, S.; Tian, S.; Ma, X. A. N.; Zhou, H.; DeYonker, N. J.; Pham, T. C.; Bollinger, J. C.; Baker, D. L.; et al. Electrocatalytic and Photocatalytic Hydrogen Production in Aqueous Solution by a Molecular Cobalt Complex. *Angew. Chem., Int. Ed.* **2012**, *51* (24), 5941−5944.

(6) Lubitz, W.; Ogata, H.; Rüdiger, O.; Reijerse, E. Hydrogenases. *Chem. Rev.* **2014**, *114* (8), 4081−4148.

(7) Lakadamyali, F.; Kato, M.; Muresan, N. M.; Reisner, E. Selective Reduction of Aqueous Protons to Hydrogen with a Synthetic Cobaloxime Catalyst in the Presence of Atmospheric Oxygen. *Angew. Chem., Int. Ed.* **2012**, *51* (37), 9381−9384.

(8) Wakerley, D. W.; Reisner, E. Oxygen-Tolerant Proton Reduction Catalysis: Much $O_2$ about Nothing? *Energy Environ. Sci.* **2015**, *8* (8), 2283−2295.

(9) Vincent, K. A.; Parkin, A.; Armstrong, F. A. Investigating and Exploiting the Electrocatalytic Properties of Hydrogenases. *Chem. Rev.* **2007**, *107* (10), 4366−4413.

(10) Plumeré, N.; Rüdiger, O.; Oughli, A. A.; Williams, R.; Vivekananthan, J.; Pöller, S.; Schuhmann, W.; Lubitz, W. A Redox Hydrogel Protects Hydrogenase from High-Potential Deactivation and Oxygen Damage. *Nat. Chem.* **2014**, *6* (9), 822−827.

(11) Fourmond, V.; Stapf, S.; Li, H.; Buesen, D.; Birrell, J.; Rüdiger, O.; Lubitz, W.; Schuhmann, W.; Plumeré, N.; Léger, C. Mechanism of Protection of Catalysts Supported in Redox Hydrogel Films. *J. Am. Chem. Soc.* **2015**, *137* (16), 5494−5505.

(12) Oughli, A. A.; Conzuelo, F.; Winkler, M.; Happe, T.; Lubitz, W.; Schuhmann, W.; Rüdiger, O.; Plumeré, N. A Redox Hydrogel Protects the $O_2$ -Sensitive [FeFe]-Hydrogenase from Chlamydomonas Reinhardtii from Oxidative Damage. *Angew. Chem., Int. Ed.* **2015**, *54* (42), 12329−12333.

(13) Oughli, A. A.; Ruff, A.; Boralugodage, N. P.; Rodríguez-Maciá, P.; Plumeré, N.; Lubitz, W.; Shaw, W. J.; Schuhmann, W.; Rüdiger, O. Dual Properties of a Hydrogen Oxidation Ni-Catalyst Entrapped within a Polymer Promote Self-Defense against Oxygen. *Nat. Commun.* **2018**, *9* (1), 864.

(14) Sakai, K.; Kitazumi, Y.; Shirai, O.; Takagi, K.; Kano, K. High-Power Formate/Dioxygen Biofuel Cell Based on Mediated Electron Transfer Type Bioelectrocatalysis. *ACS Catal.* **2017**, *7* (9), 5668−5673.

(15) Ruff, A.; Szczesny, J.; Zacarias, S.; Pereira, I. A. C.; Plumeré, N.; Schuhmann, W. Protection and Reactivation of the [NiFeSe] Hydrogenase from Desulfovibrio Vulgaris Hildenborough under Oxidative Conditions. *ACS Energy Lett.* **2017**, *2* (5), 964−968.

(16) Liebgott, P.-P.; de Lacey, A. L.; Burlat, B.; Cournac, L.; Richaud, P.; Brugna, M.; Fernandez, V. M.; Guigliarelli, B.; Rousset, M.; Léger, C.; et al. Original Design of an Oxygen-Tolerant [NiFe] Hydrogenase: Major Effect of a Valine-to-Cysteine Mutation near the Active Site. *J. Am. Chem. Soc.* **2011**, *133* (4), 986−997.

(17) Schröder, V.; Emonts, B.; Janßen, H.; Schulze, H.-P. Explosion Limits of Hydrogen/Oxygen Mixtures at Initial Pressures up to 200 bar. *Chem. Eng. Technol.* **2004**, *27* (8), 847−851.

(18) Li, H.; Münchberg, U.; Lubitz, W.; Freier, E.; Plumeré, N. Suppressing $H_2O_2$ Generation to Achieve $O_2$-Insensitivity of a [NiFe] Hydrogenase in Redox Active Films. *Nat. Commun.* **2019**, submitted.

(19) Liebhafsky, H. A. The catalytic decomposition of hydrogen peroxide by the iodine-iodide couple at 25°. *J. Am. Chem. Soc.* **1932**, *54* (5), 1792−1806.

(20) Li, H.; Buesen, D.; Williams, R.; Henig, J.; Stapf, S.; Mukherjee, K.; Freier, E.; Lubitz, W.; Winkler, M.; Happe, T.; et al. Preventing the Coffee-Ring Effect and Aggregate Sedimentation by in Situ Gelation of Monodisperse Materials. *Chem. Sci.* **2018**, *9* (39), 7596−7605.

(21) Léger, C.; Dementin, S.; Bertrand, P.; Rousset, M.; Guigliarelli, B. Inhibition and Aerobic Inactivation Kinetics of Desulfovibrio Fructosovorans NiFe Hydrogenase Studied by Protein Film Voltammetry. *J. Am. Chem. Soc.* **2004**, *126* (38), 12162−12172.

(22) Bartlett, P. N.; Pratt, K. F. E. Theoretical Treatment of Diffusion and Kinetics in Amperometric Immobilized Enzyme Electrodes Part I: Redox Mediator Entrapped within the Film. *J. Electroanal. Chem.* **1995**, *397* (1−2), 61−78.

(23) Abou Hamdan, A.; Burlat, B.; Gutiérrez-Sanz, O.; Liebgott, P.-P.; Baffert, C.; De Lacey, A. L.; Rousset, M.; Guigliarelli, B.; Léger, C.; Dementin, S. $O_2$-Independent Formation of the Inactive States of NiFe Hydrogenase. *Nat. Chem. Biol.* **2013**, *9* (1), 15−17.

(24) Abou Hamdan, A.; Liebgott, P.-P.; Fourmond, V.; Gutiérrez-Sanz, O.; De Lacey, A. L.; Infossi, P.; Rousset, M.; Dementin, S.; Léger, C. Relation between Anaerobic Inactivation and Oxygen Tolerance in a Large Series of NiFe Hydrogenase Mutants. *Proc. Natl. Acad. Sci. U. S. A.* **2012**, *109* (49), 19916−19921.

(25) Del Barrio, M.; Sensi, M.; Orain, C.; Baffert, C.; Dementin, S.; Fourmond, V.; Léger, C. Electrochemical Investigations of Hydrogenases and Other Enzymes That Produce and Use Solar Fuels. *Acc. Chem. Res.* **2018**, *51* (3), 769−777.

(26) Volbeda, A.; Martin, L.; Liebgott, P.-P.; De Lacey, A. L.; Fontecilla-Camps, J. C. [NiFe]-Hydrogenases Revisited: Nickel-Carboxamido Bond Formation in a Variant with Accrued $O_2$-Tolerance and a Tentative Re-Interpretation of Ni-SI States. *Metallomics* **2015**, *7* (4), 710−718.

(27) Bird, C. L.; Kuhn, A. T. Electrochemistry of the Viologens. *Chem. Soc. Rev.* **1981**, *10* (1), 49.

(28) Cracknell, J. A.; Wait, A. F.; Lenz, O.; Friedrich, B.; Armstrong, F. A. A Kinetic and Thermodynamic Understanding of $O_2$ Tolerance in [NiFe]-Hydrogenases. *Proc. Natl. Acad. Sci. U. S. A.* **2009**, *106* (49), 20681−20686.

(29) Pandelia, M.-E.; Fourmond, V.; Tron-Infossi, P.; Lojou, E.; Bertrand, P.; Léger, C.; Giudici-Orticoni, M.-T.; Lubitz, W. Membrane-Bound Hydrogenase I from the Hyperthermophilic Bacterium Aquifex Aeolicus: Enzyme Activation, Redox Intermediates and Oxygen Tolerance. *J. Am. Chem. Soc.* **2010**, *132* (20), 6991−7004.

(30) Morozov, S.; Voronin, O.; Karyakina, E.; Zorin, N.; Cosnier, S.; Karyakin, A. Tolerance to Oxygen of Hydrogen Enzyme Electrodes. *Electrochem. Commun.* **2006**, *8* (5), 851−854.

(31) Wait, A. F.; Parkin, A.; Morley, G. M.; dos Santos, L.; Armstrong, F. A. Characteristics of Enzyme-Based Hydrogen Fuel Cells Using an Oxygen-Tolerant Hydrogenase as the Anodic Catalyst. *J. Phys. Chem. C* **2010**, *114* (27), 12003−12009.

(32) Wulff, P.; Thomas, C.; Sargent, F.; Armstrong, F. A. How the oxygen tolerance of a [NiFe]-hydrogenase depends on quaternary structure. *JBIC, J. Biol. Inorg. Chem.* **2016**, *21* (1), 121−134.

(33) Radu, V.; Frielingsdorf, S.; Evans, S. D.; Lenz, O.; Jeuken, L. J. C. Enhanced oxygen-tolerance of the full heterotrimeric membrane-bound [NiFe]-hydrogenase of Ralstonia eutropha. *J. Am. Chem. Soc.* **2014**, *136* (24), 8512−8515.

(34) Yang, X.; Elrod, L. C.; Reibenspies, J. H.; Hall, M. B.; Darensbourg, M. Y. Oxygen Uptake in Complexes Related to [NiFeS]- and [NiFeSe]-Hydrogenase Active Sites. *Chem. Sci.* **2019**, *10* (5), 1368−1373.




DOI: 10.1021/jacs.9b06790
*J. Am. Chem. Soc.* 2019, 141, 16734−16742